

DISK-SATELLITE INTERACTION IN DISKS WITH DENSITY GAPS

CRISTOBAL PETROVICH¹ & ROMAN R. RAFIKOV^{1,2}
Draft version July 9, 2018

ABSTRACT

Gravitational coupling between a gaseous disk and an orbiting perturber leads to angular momentum exchange between them which can result in gap opening by planets in protoplanetary disks and clearing of gas by binary supermassive black holes (SMBHs) embedded in accretion disks. Understanding the co-evolution of the disk and the orbit of the perturber in these circumstances requires knowledge of the spatial distribution of the torque exerted by the latter on a highly nonuniform disk. Here we explore disk-satellite interaction in disks with gaps in linear approximation both in Fourier and in physical space, explicitly incorporating the disk non-uniformity in the fluid equations. Density gradients strongly displace the positions of Lindblad resonances in the disk (which often occur at multiple locations), and the waveforms of modes excited close to the gap edge get modified compared to the uniform disk case. The spatial distribution of the excitation torque density is found to be quite different from the existing prescriptions: most of the torque is exerted in a rather narrow region near the gap edge where Lindblad resonances accumulate, followed by an exponential fall-off with the distance from the perturber. Despite these differences, for a given gap profile the full integrated torque exerted on the disk agrees with the conventional uniform disk theory prediction at the level of $\sim 10\%$. The nonlinearity of the density wave excited by the perturber is shown to decrease as the wave travels out of the gap, slowing down its nonlinear evolution and damping. Our results suggest that gap opening in protoplanetary disks and gas clearing around SMBH binaries can be more efficient than the existing theories predict. They pave the way for self-consistent calculations of the gap structure and the orbital evolution of the perturber using accurate prescription for the torque density behavior.

Subject headings: accretion, accretion disks — instabilities — (stars:) planetary systems: protoplanetary disks — (galaxies:) quasars: general

1. INTRODUCTION.

Gravitational coupling between a gaseous disk and an external orbiting body plays an important role in many astrophysical systems, including disk-planet interaction in protoplanetary disks, orbital evolution of supermassive black hole (SMBH) binaries surrounded by gaseous disks, dynamics of accretion disks in cataclysmic variables, and so on. This interaction leads to angular momentum exchange between the disk and the perturber, causing the orbit of the latter to evolve — an effect responsible for the planet migration in protoplanetary disks (Ward 1986, 1997) and the black hole inspiral in the case of SMBH binaries embedded in gaseous disks (Ivanov et al. 1999; Gould & Rix 2000)

Tidal disk-satellite³ coupling also modifies the distribution of the gas surface density and can result in gap opening in protoplanetary disks (Ward 1997) and cavity formation around the SMBH binaries (Armitage et al. 2002) if the perturber is massive enough. Gap opening necessarily weakens the tidal coupling between the perturber and the disk, and slows the orbital migration of the perturber, switching it to the so-called Type II regime, (Ward 1986). Thus, gap opening can be an important “parking mechanism” preventing massive plan-

ets from migrating all the way to the central star.

In steady state the gap structure is determined by the local balance between the planetary torque acting on the disk and the divergence of the external stress $T_{r\varphi}$, which can be due to magnetorotational instability or some other mechanism of intrinsic angular momentum transport in the disk:

$$\left. \frac{dT}{dr} \right|_d = \frac{dT_{r\varphi}}{dr}. \quad (1)$$

Here $dT/dr|_d$ is the torque density (the amount of torque per unit radial distance) *deposited in the disk* by the density waves originally launched by the planetary tide closer to the planet. The deposition of the wave angular momentum in the disk occurs by virtue of some linear (Takeuchi et al. 1996) or nonlinear (Goodman & Rafikov 2001) *damping* process. In general the spatial distribution of $dT/dr|_d$ can be described as

$$\left. \frac{dT}{dr} \right|_d = \mathcal{L} * \left(\frac{dT}{dr} \right), \quad (2)$$

where the intrinsically non-local operator \mathcal{L} describes the wave damping, and dT/dr is the *excitation* torque density — the rate at which planetary potential adds angular momentum to the propagating density waves per unit radial distance.

Thus, in order to understand the details of gap opening one must understand both the *excitation* of waves and their *damping*, a key point first highlighted

¹ Department of Astrophysical Sciences, Princeton University, Ivy Lane, Princeton, NJ 08540; rrr@astro.princeton.edu

² Sloan Fellow

³ We will refer as disk-satellite or disk-planet to any type of system where the tidal coupling is present, e.g., an SMBH binary surrounded by the disk, an accreting white dwarf-main sequence star binary, etc.

by Lunine & Stevenson (1982), Greenberg (1983), and Goldreich & Nicholson (1989). Once the description of the wave damping (i.e. the explicit form of the operator \mathcal{L}) is available, the steady state gap structure is fully determined by the spatial structure of the excitation torque density dT/dr .

In this work, following the approach of Rafikov & Petrovich (2012; hereafter RP12) we concentrate only on the process of wave excitation, which at least in some cases (Goodman & Rafikov 2001) can be studied separately from the wave dissipation (when the latter is weak). Our goal is to provide a self-consistent calculation of the excitation torque density dT/dr in *non-uniform* disks affected by gap formation. Prior to this work the majority of existing studies of the gap and cavity opening in disks have adopted the following simple prescription for the excitation torque density behavior in non-uniform disks:

$$\frac{dT(r)}{dr} = \frac{\Sigma(r)}{\Sigma_0} \left. \frac{dT(r)}{dr} \right|_u, \quad (3)$$

where $dT/dr|_u$ is the excitation torque density in a *uniform* disk with surface density Σ_0 , and $\Sigma(r)$ is the spatially varying surface density in a non-uniform disk.

The behavior of $dT/dr|_u$ has been previously derived from direct numerical simulations (Bate et al. 2003; de Val-Borro et al. 2006; D’Angelo & Lubow 2008, 2010; Dong et al. 2011a,b) and from analytical linear studies (GT80; Muto & Inutsuka 2009; RP12). In particular, in their pioneering study of disk-satellite interaction Goldreich & Tremaine (1980) have shown that far from the perturber, at radial separations from its orbit $|r - r_p|$ (r_p is the semimajor axis of the circular orbit of the planet) exceeding the disk scale height h , the uniform disk excitation torque density⁴ $dT/dr|_u$ is given by

$$\left. \frac{dT}{dr} \right|_u \rightarrow \text{sign}(r - r_p) C_{GT80} \frac{(GM_p)^2 \Sigma_0}{\Omega^2 |r - r_p|^4},$$

$$C_{GT80} = \frac{32}{81} \left[2K_0 \left(\frac{2}{3} \right) + K_1 \left(\frac{2}{3} \right) \right]^2 \approx 2.5, \quad (4)$$

where M_p is the planetary mass, Σ_0 is the disk surface density assumed to be uniform on scales $\sim |r - r_p|$, Ω is the angular frequency of the disk at r_p , and K_n is the modified Bessel function of order n . Note that strictly speaking dT/dr in equation (4) represents the *force density* and not the angular momentum density as it lacks an additional factor of r_p . This is because our subsequent calculations are cast in the shearing sheet framework in which the concept of r_p is not well defined.

The general scaling $dT/dr|_u \propto |r - r_p|^{-4}$ has been also confirmed by Lin & Papaloizou (1979) using impulse approximation. A number of studies of gap opening by planets (Lin & Papaloizou 1986; Trilling et al. 1998; Bryden et al. 1999; Armitage et al. 2002; Varnière et al. 2004; Crida et al. 2006) and orbital evolution of SMBH binaries surrounded by gaseous disks (Gould & Rix 2000; Armitage & Natarajan 2002; Lodato et al. 2009;

Alexander et al. 2011) have used the prescription⁵ (3) combined with asymptotic GT80 formula (4) for $dT/dr|_u$, in some cases with a value of the constant pre-factor different from C_{GT80} (Papaloizou & Lin 1984; Armitage & Natarajan 2002).

Recently, Dong et al. (2011a) carried out high-resolution numerical simulations of disk-planet interaction in the two-dimensional shearing sheet geometry. Contrary to the prediction (4) of GT80 they found that the one-sided excitation torque density $dT/dr|_u$ does not maintain a fixed sign but rather changes from positive to negative at a distance of $\approx 3.2h$ from the perturber — a result recently confirmed by global simulations of Duffell & MacFadyen (2012). This negative torque density phenomenon was then explained analytically in the framework of linear theory by RP12, who traced its origin to the overlap of Lindblad resonances in the vicinity of the perturber’s orbit (which was ignored in GT80).

This unexpected finding casts serious doubt on the validity of simple prescription (3) in non-uniform disks. Indeed, directly substituting $dT/dr|_u$ computed by RP12 in equation (3) can result in *negative* total torque exerted on the disk by the perturber if the gap is sufficiently wide and deep (in view of RP12 results this is certainly true in the extreme case of the gas density being exactly zero at separations less than $3.2h$ from the planetary orbit). This conclusion is unphysical (planet would not open a gap in the first place), suggesting that the oversimplified prescription (3) incorporating the disk non-uniformity only through the direct multiplication by the local surface density (so that density *gradients* do not affect disk-satellite coupling) needs to be revised.

In this work, we provide a fully self-consistent linear calculation of the disk-satellite interaction by explicitly incorporating the disk non-uniformity in the fluid equations and properly accounting for the effect of density gradients on the waveforms of perturbed fluid variables. In this way we are able to compute the torque density and angular momentum flux in Fourier and physical space and demonstrate significant differences with the results obtained using the prescription (3), especially at the gap edges where the density gradients are large.

Our paper is structured as follows. In §2 we describe the problem setup, in particular the governing equations, the assumed gap density profile, and the Lindblad resonances in non-uniform disks. Our numerical procedure and the results for the density wave behavior are described in §3. Calculations of the torque exerted by the perturber on the disk in Fourier and real space are described in §5 and 6, respectively. Finally, we discuss our results, including their astrophysical applications, in §8.

2. PROBLEM SETUP.

We start by deriving a system of linearized equations and describing the adopted underlying surface density distribution — the ingredients needed to calculate the spatial behavior of the perturbed quantities.

2.1. Basic equations.

⁴ We assume that GT80 calculation refers to dT/dr and not to $dT/dr|_a$ since no explicit dissipation mechanism was mentioned in their work.

⁵ It should also be pointed out that in all these studies the excitation torque density dT/dr was identified with the deposition torque density $dT/dr|_a$, thus ignoring the process of wave dissipation altogether, see equation (2).

We study the tidal coupling of a planet with a non-uniform disk in the shearing sheet geometry (Goldreich & Lynden-Bell 1965), which allows us to neglect geometric curvature effects while preserving the main qualitative features of the system. We also neglect the vertical dimension and assume the disk to be two-dimensional. The dynamics of fluid is then governed by the following equations⁶ (e.g. Narayan et al. 1987; hereafter NGG):

$$\frac{\partial \mathbf{v}}{\partial t} + (\mathbf{v} \cdot \nabla) \mathbf{v} + 2\boldsymbol{\Omega} \times \mathbf{v} + 4A\Omega x \mathbf{e}_x = -\frac{\nabla P}{\Sigma} - \nabla \Phi_p \quad (5)$$

$$\frac{\partial \Sigma}{\partial t} + \nabla \cdot (\mathbf{v}\Sigma) = 0, \quad (6)$$

where $\mathbf{v} = (u, v)$ is the fluid velocity with components in the $x \equiv r - r_p$ (radial) and y (azimuthal) directions correspondingly, P is gas pressure, Φ_p is the planetary potential, $\boldsymbol{\Omega}_p \equiv \Omega_p \mathbf{e}_z$ is the Keplerian rotation frequency at the planet position ($r = r_p$; we will subsequently drop the subscript ‘‘p’’ for brevity), and $A \equiv (r/2)(d\Omega/dr)$ is the shear rate at the same location. Additionally, in our notation c_s is the sound speed and $B = \Omega + A$ is Oort’s B constant.

For an isothermal disk with no planet present ($\phi \equiv 0$) and for an arbitrary background density profile $\Sigma = \Sigma_0(x)$, the Equations (5) and (6) have the following exact steady-state solution

$$u_0 = 0, \quad v_0 = 2Ax + \frac{c_s^2}{2\Omega} \frac{\partial \ln \Sigma_0}{\partial x}. \quad (7)$$

After having specified our steady-state solution $\{\Sigma_0, u_0, v_0\}$, we introduce the planetary potential as a perturbation and study the linear behavior of the perturbed density Σ_1 and velocity field $\delta \mathbf{v} = (u_1, v_1)$. By ignoring the quadratic perturbed quantities that appear in the Equations (5) and (6) one can get the following general system

$$\frac{\partial u_1}{\partial t} + \left(2Ax + \frac{c_s^2}{2\Omega} \frac{\partial \ln \Sigma_0}{\partial x}\right) \frac{\partial u_1}{\partial y} - 2\Omega v_1 + \frac{c_s^2}{\Sigma_0} \frac{\partial (\Sigma_1/\Sigma_0)}{\partial x} = -\frac{\partial \Phi_p}{\partial x} \quad (8)$$

$$\frac{\partial v_1}{\partial t} + \left(2Ax + \frac{c_s^2}{2\Omega} \frac{\partial \ln \Sigma_0}{\partial x}\right) \frac{\partial v_1}{\partial y} + \left(2B + \frac{c_s^2}{2\Omega} \frac{\partial^2 \ln \Sigma_0}{\partial x^2}\right) u_1 + c_s^2 \frac{\partial (\Sigma_1/\Sigma_0)}{\partial y} = -\frac{\partial \Phi_p}{\partial y} \quad (9)$$

$$\frac{\partial (\Sigma_1/\Sigma_0)}{\partial t} + \left(2Ax + \frac{c_s^2}{2\Omega} \frac{\partial \ln \Sigma_0}{\partial x}\right) \frac{\partial (\Sigma_1/\Sigma_0)}{\partial y} + u_1 \frac{\partial \ln \Sigma_0}{\partial x} + \frac{\partial u_1}{\partial x} + \frac{\partial v_1}{\partial y} = 0 \quad (10)$$

We then represent all perturbed fluid variables via Fourier integrals as $\{\Sigma_1, u_1, v_1, \Phi_p\} = (2\pi)^{-1} \int_{-\infty}^{\infty} \exp(ik_y y) \{\delta \Sigma, u, v, \phi\}$, which takes care of the y -dependence leaving us with the following set of

⁶ Analogous equation (3) in RP12 has a typo: the term $4A\Omega z \mathbf{e}_x$ should be $4A\Omega x \mathbf{e}_x$. This typo does not affect any other part of the paper.

equations in the x -coordinate only. Thus, by defining

$$\sigma(x) = -2Ak_y x - \frac{c_s^2 k_y}{2\Omega} \frac{\partial \ln \Sigma_0}{\partial x}, \quad (11)$$

$$\tilde{B} = B + \frac{c_s^2}{4\Omega} \frac{\partial^2 \ln \Sigma_0}{\partial x^2} \quad (12)$$

we get the linearized system in steady state ($\partial/\partial t \equiv 0$)

$$-i\sigma u - 2\Omega v + c_s^2 \frac{\partial (\delta \Sigma/\Sigma_0)}{\partial x} = -\frac{\partial \phi}{\partial x} \quad (13)$$

$$-i\sigma v + 2\tilde{B}u + ik_y c_s^2 \frac{\delta \Sigma}{\Sigma_0} = -ik_y \phi \quad (14)$$

$$-i\sigma \frac{\delta \Sigma}{\Sigma_0} + u \frac{\partial \ln \Sigma_0}{\partial x} + \frac{\partial u}{\partial x} + ik_y v = 0, \quad (15)$$

where the Fourier component of the planetary potential produced by a point mass at the origin and its derivative are given by

$$\phi(k_y, x) = -\frac{GM_p}{\pi} K_0(|k_y x|), \quad (16)$$

$$\frac{\partial \phi}{\partial x} = \text{sgn}(x) \frac{GM_p}{\pi} k_y K_1(|k_y x|). \quad (17)$$

Solving (13)-(15) for the azimuthal velocity perturbation v , we obtain the second order ordinary differential equation

$$\frac{\partial^2 v}{\partial x^2} + \frac{\partial v}{\partial x} \frac{\partial \ln(\Sigma_0/\Delta)}{\partial x} + v \left[\frac{\sigma^2}{c_s^2} - \frac{\Omega}{c_s^2 \tilde{B}} \Delta + \frac{k_y \sigma \Lambda}{2\tilde{B}} \frac{\partial \ln(\sigma \Lambda/\Delta)}{\partial x} \right] = -\frac{\partial \phi}{\partial x} \frac{2\tilde{B}}{c_s^2} + \phi \left[\frac{k_y \sigma}{c_s^2} + \frac{k_y^2 \Lambda}{2\tilde{B}} \frac{\partial \ln(\Lambda/\Delta)}{\partial x} \right], \quad (18)$$

where we have defined

$$\Lambda = 1 - \frac{2}{k_y \sigma} \left(\frac{\partial \tilde{B}}{\partial x} - \tilde{B} \frac{\partial \ln \Sigma_0}{\partial x} \right), \quad (19)$$

$$\Delta = c_s^2 k_y^2 \Lambda + 4\tilde{B}^2. \quad (20)$$

The perturbed radial velocity u and the surface density perturbation $\delta \Sigma$ are directly expressed in terms of v via the following relations:

$$u = -\frac{i}{\Delta} \left(k_y c_s^2 \frac{\partial v}{\partial x} - 2\tilde{B} \sigma v + 2\tilde{B} k_y \phi \right), \quad (21)$$

$$\delta \Sigma = \frac{\Sigma_0}{\Delta} \left(2\tilde{B} \frac{\partial v}{\partial x} + k_y \sigma \Lambda v - k_y^2 \Lambda \phi \right). \quad (22)$$

One can easily check that in the limit $\partial \Sigma_0/\partial x \rightarrow 0$ equation (18) reduces to equation (5) of RP12 which was derived for a uniform disk.

2.2. Disk models

We model the density structure of an axisymmetric gap around the satellite orbit by a particular three parameter density profile (symmetric with respect to $x = 0$)

$$\frac{\Sigma_0(x)}{\Sigma_\infty} = 1 - \frac{1 - \Sigma_{\min}}{1 + (x/\delta)^n \exp\left[-(2.5\delta/x)^2\right]}, \quad (23)$$

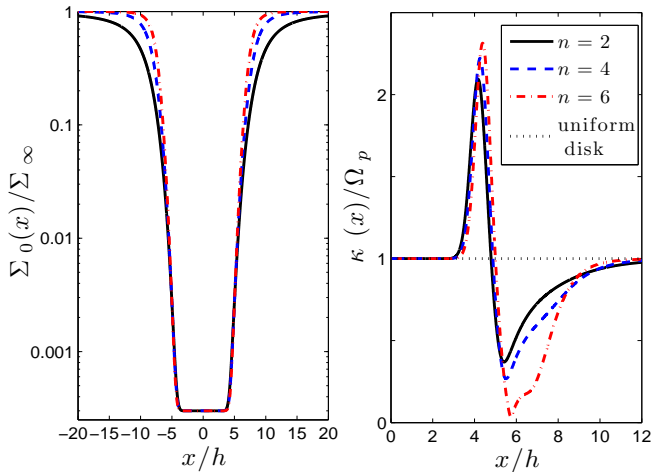


FIG. 1.— Density profiles (left panel) and epicyclic frequencies κ (right panel) for the gap models described by Eq. (23) with parameters $\delta = 5h$, $\Sigma_{\min} = 3 \times 10^{-4}$, and $n = 2, 4, 6$.

where the surface density is normalized to its value at infinity Σ_{∞} . In this profile the dimensionless parameter Σ_{\min} controls the depth of the gap, δ regulates its width, while an even positive integer n sets the steepness of the density gradient at the gap edge. The density variation between $\Sigma_{\min}\Sigma_{\infty}$ inside the gap and Σ_{∞} outside of it is predominantly due to the power law dependence on x in the denominator of the second term in the right hand side of the equation (23). The exponential dependence in the denominator is introduced only to ensure a flat bottom at $x \lesssim \delta$ and allows us to avoid large density gradients close to the origin. This simplifies our subsequent analysis and helps us get important contributions to the torque from just outside the gap, exactly where we want to test our theory. The factor 2.5 in the exponential is introduced for the parameter δ to better correspond to the width of the inner, flat part of the gap.

In the left panel of Figure 1 we plot the density profile for the disk model with parameters $\delta = 5h$, $\Sigma_{\min} = 3 \times 10^{-4}$, and with $n = 2, 4, 6$, respectively. These profiles represent rather broad gaps: for the models with $\delta = 5h$ shown in Figure 1 one finds that the density $\Sigma_{\infty}/2$ is reached at $|x| \approx 10h$, $|x| \approx 8.5h$, and $|x| \approx 7.7h$ for $n = 2, 4$, and 6 respectively. Evidently, as n is increased the profile becomes boxier and the gradients at the gap edge (they are largest for $4h \lesssim |x| \lesssim 15h$) grow.

2.3. Shifted Lindblad resonances

Non-zero pressure gradients intrinsic to inhomogeneous disks affect the unperturbed azimuthal velocity (7) and change the locations of the Lindblad resonances, at which different harmonics of planetary potential couple to the disk, compared to the purely Keplerian case. In Appendix A we demonstrate that in the shearing sheet approximation a given k_y harmonic has Lindblad resonance condition satisfied at $x_L(k_y)$ satisfying the following implicit relation:

$$k_y(x_L) = \pm \frac{2}{3} \frac{\kappa(x_L)}{\Omega_p} \left(x_L - \frac{h^2}{3} \frac{\partial \ln \Sigma_0}{\partial x} \Big|_{x_L} \right)^{-1}, \quad (24)$$

where the modified value of the local epicyclic frequency κ for the inhomogeneous disk is given by (see Appendix

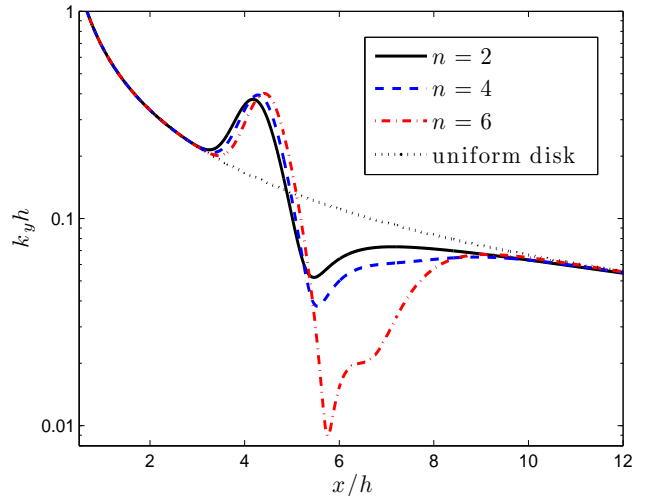


FIG. 2.— Azimuthal wavenumber k_y as a function of the Lindblad resonance position given by Eq. (24) for the surface profile described by Eq. (23) with parameters $\delta = 5h$, $\Sigma_{\min} = 3 \times 10^{-4}$, and $n = 2, 4, 6$. The dotted line indicates the uniform disk case $k_y = 2/(3x)$ for comparison.

A)

$$\kappa(x) = \Omega_p \left(1 + h^2 \frac{\partial^2 \ln \Sigma_0}{\partial x^2} \right)^{1/2}. \quad (25)$$

In a uniform disk ($\partial \ln \Sigma_0 / \partial x = 0$) one recovers the usual expressions $\kappa = \Omega_p$ and $x_L(k_y) = 2/(3k_y)$.

For a class of density profiles (23) considered in this work the modification to the $x_L(k_y)$ relation (24) compared to the purely Keplerian case comes predominantly from the change of the local epicyclic frequency as given by equation (25). For this reason we explore the dependence of κ on x in some detail and plot it in the right panel of Figure 1 for the density profiles shown in the left panel of the same Figure.

Deep inside the gap Σ_0 is almost constant because of the assumed exponential dependence in equation (23) and $\kappa(x) \rightarrow \Omega_p$. As the gap edge is approached, at $|x| \gtrsim 4h$, $\partial^2 \ln \Sigma_0 / \partial x^2$ increases and κ does the same: in all displayed models κ goes up to $\gtrsim 2\Omega_p$. Beyond $|x| \gtrsim 5h$ the density profiles change their curvature from positive to negative and κ becomes smaller than Ω_p . At even larger $|x|$ the density profile flattens out and κ converges to Ω_p at $|x| \gtrsim 15h$. The deviations of the epicyclic frequency compared to its value in a uniform disk become more extreme as we increase n (increase boxiness of $\Sigma_0(x)$), with the differences between models being more dramatic in regions where $\kappa < \Omega_p$. The minimum values of κ are $0.36\Omega_p$, $0.27\Omega_p$, and $0.03\Omega_p$ for profiles with $n = 2, 4$, and 6 , respectively, see Figure 1.

In fact, one can see from equation (25) that depending on the curvature of Σ_0 the gap profile could have $\kappa^2 < 0$ at the gap edge, which would mean that the disk is Rayleigh unstable. For this reason in this work we ignore profiles with extremely deep gaps and strong density gradients at their edges since these are likely to result in $\kappa^2 < 0$ at some place. Our boxiest model with $n = 6$ might be regarded as a limiting profile (for assumed values of δ and Σ_{\min}) since the epicyclic frequency closely approaches zero at $x \approx 6h$.

Armed with this knowledge we plot in Figure 2 the dependence (24) for the density model given by equation (23) with the same set of parameters as in Figure 1: $\delta = 5h$, $\Sigma_{\min} = 3 \times 10^{-4}$, and $n = 2, 4, 6$. By comparing these two Figures one can see that the resonances are displaced *outwards* relative to the uniform density case in regions where $\kappa > \Omega_p$, while the opposite happens when $\kappa < \Omega_p$. As a result, there is a *concentration of the resonances* at the gap edge where this transition occurs.

Indeed, in a uniform disk with $\kappa = \Omega_p$ the radial interval $4h < |x| < 6h$ contains Lindblad resonances only for the modes with $k_y h$ in the range (0.11, 0.17). At the same time, for the gap in the form (23) with $n = 2$ the same radial interval contains Lindblad resonances for modes satisfying $0.05 \lesssim k_y h \lesssim 0.37$; for $n = 6$ model modes with $0.009 \lesssim k_y h \lesssim 0.4$ are being excited in the same radial interval. Thus, concentration of resonances at the gap edge is more pronounced for density profiles with larger gradients meaning larger deviations of κ from Ω_p .

Another striking feature of the $x_L(k_y)$ dependence clearly visible in Figure 2 is that even for not very sharp gaps (for rather low values of n) there are regions close to the gap edge where a single k_y mode can be excited at two or three different locations (for a fixed sign of x), as happens e.g. for $k_y h = 0.3$ in this Figure. This splitting of resonances in inhomogeneous disks has important implications for the torque behavior in Fourier space, see §5.

3. NUMERICAL RESULTS

3.1. Numerical procedure.

Having specified the gap density profile the solution for the azimuthal velocity perturbation v is obtained by direct numerical integration of the equations (11), (12), (16)-(20); knowing v we find u and $\delta\Sigma$ using equations (21), (22).

Numerical integration uses the same method as was employed in RP12 for uniform disks: we shoot numerical solutions from the origin and match them to the WKB outgoing waves far from the planet (see also Korycansky & Pollack (1993)). As shown in NGG, the exact homogeneous solution to Equation (18) for a homogeneous disk, i.e. the parabolic cylinder functions, can be well approximated by the WKB outgoing waves

$$v(x \rightarrow \pm\infty) \sim \sqrt{\frac{2}{3k_y x}} e^{\pm i3k_y x^2/4h} \quad (26)$$

when $x/h \gg (8/9)[1 + (k_y h)^2]/(k_y h)^2$. Moreover, for this approximation to accurately represent an inhomogeneous solution of Equation (18) one requires $xk_y \gg 1$, so that $\phi \ll 1$ and $\partial\phi/\partial x \ll 1$.

To additionally account for the presence of a density gap in the disk, we use the fact that for every profile $\partial\Sigma_0/\partial x \rightarrow 0$ when x is several times the characteristic width of the gap δ and, therefore, the asymptotic solution will still be given by (26). All conditions together imply that $x/h \gg \min\{1/(k_y h), 1, \delta/h\}$, which is the criterion we use to match our numerical solutions to the outgoing waves.

Our numerical calculations use a 4-th order Runge-Kutta integrator with spatial resolution of $h/400$ and $x \in [-220h, 220h]$ for 720 uniformly log-spaced values of

$k_y h$ between 0.01 and 15, and potential softening length of $10^{-4}h$.

3.2. Density wake

In Figure 3 we show one of the outcomes of our calculations — the behavior of the surface density perturbation $\Sigma_1(x, y)$ in physical space. We obtain it by first calculating $\delta\Sigma$ using Equation (22) with the numerically determined v and then performing the inverse Fourier transform. In Figure 3 azimuthal cuts of $\Sigma_1(x, y)$ at different values of x are normalized by $(\Sigma_0(x)x)^{1/2}$ to ensure similar wake amplitude at different radial separations from the perturber; this scaling is expected⁷ from the conservation of the angular momentum flux carried by the density wave (Goodman & Rafikov 2001; Rafikov 2002a).

In panel (a) we display our results for a shallow gap with a minimum surface density at the satellite position of $0.1\Sigma_\infty$ (corresponding density profile is shown in panel (b)). For comparison we also display the wake profiles for a uniform density disk. Deep inside the gap, at $x = h$, where the Σ_0 is essentially constant in our model we find our Σ_1 to exactly coincide with the uniform disk calculation, as expected (our normalization of Σ_1 takes care of the difference in amplitude). However, further out from the planet the results start to differ. In particular, at $x = 10h$ the azimuthal location of the wake in a non-uniform disk gets shifted by $\approx h$ relative to the uniform case, but the differences in the shape of the density perturbation remain at the modest level.

Situation is a bit different for deep gaps, as illustrated in panel (c) where we plot azimuthal density cuts through the wake for a gap profile with $\Sigma_{\min} = 0.0003\Sigma_\infty$ (shown in panel (d)). Again, at $x = h$ density profiles coincide for both uniform and non-uniform cases. However, at the gap edge (at $x = 5h$) there are now substantial differences between the profiles not only in the wake position but also in shape. The differences become more pronounced as the wave propagates even further: at $x = 10h$ the peak value of Σ_1 is shifted by $\sim 4h$ compared to the uniform case and the overall wake shape is considerably distorted. This is not surprising since the surface density eigenfunctions at the edge of the gap in a non-uniform disk are considerably distorted compared to their uniform disk analogues, see §5.1.

Note that the amplitude of scaled Σ_1 in Figure 3 does not vary too much with x . Since the angular momentum flux conservation predicts that $\Sigma_1 \propto [\Sigma_0(x)x]^{1/2}$ it is clear that the amplitude of Σ_1 *grows* as the wake propagates out from the bottom of the gap. At the same time, the relative density perturbation $\Sigma_1/\Sigma_0(x)$ scales as $[x/\Sigma_0(x)]^{1/2}$ and *decreases* as the wake climbs up the density contrast at the gap edge. This may have important implications for the wake damping, as discussed in §8.

4. ANGULAR MOMENTUM TRANSPORT: PRELIMINARIES

One of the key characteristics of the disk-satellite coupling is the excitation torque density dT/dx (or equiva-

⁷ This expectation is only approximate since the angular momentum flux carried by the wake can vary substantially across the gap edge, see §6.2. Nevertheless, the proposed scaling works quite well in practice, which is obvious from Figure 3.

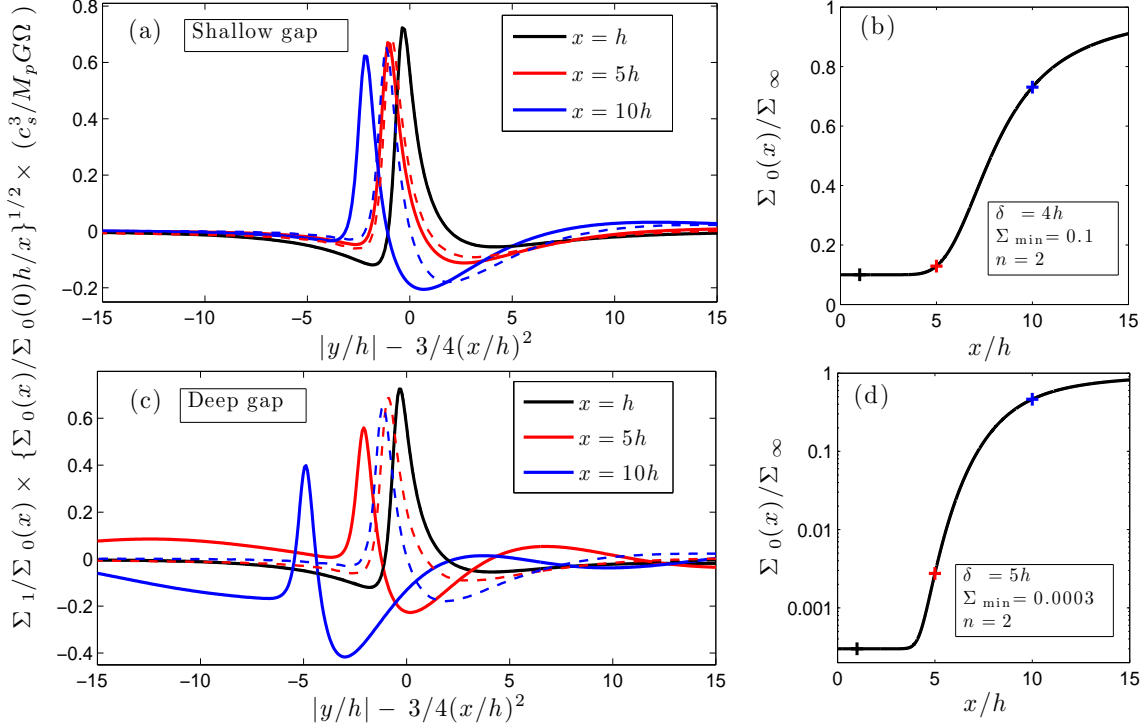


FIG. 3.— Azimuthal cuts through the density wake in coordinate space showing the density perturbation $\Sigma_1(x, y)$ at different radial separations from the satellite ($x = h, 5h, 10h$ as labeled), normalized by $[\Sigma_0(x)]^{1/2}$, and azimuthally shifted by $(3/4)x^2$ to facilitate comparison. The solid lines in panels (a) and (c) show the results for the shallow gap profile (panel b; Eq. (23) with $\delta = 4h$, $\Sigma_{\min} = 0.1$, $n = 2$) and deep profile (panel d; $\delta = 5h$, $\Sigma_{\min} = 3 \times 10^{-4}$, and $n = 2$), respectively, while the dashed lines are results for a uniform disk shown in left panels. Marks on the density profiles in right panels indicate the radial position of the azimuthal cuts shown in left panels.

lently dT/dr) — the amount of the angular momentum added by the satellite tide to the density wave per unit radial distance x . Following RP12 we express it via the imaginary part of the density perturbation $\Im(\delta\Sigma)$ as

$$\frac{dT}{dx} = \int_{-\infty}^{\infty} dy \delta\Sigma \frac{\partial\Phi}{\partial y} = \int_0^{\infty} \left(\frac{dT}{dx} \right)_{k_y} dk_y, \quad (27)$$

$$\left(\frac{dT}{dx} \right)_{k_y} = -4\pi k_y \phi \Im(\delta\Sigma), \quad (28)$$

where $(dT/dx)_{k_y}$ is the torque density contribution due to mode with wavenumber k_y . Integrated (one-sided) torque is then defined as $T(x) = \int_0^x (\partial T/\partial x') dx'$. Note that in the shearing sheet approximation there is no net torque and $T(x) = -T(-x)$.

Integrated torque is closely related to the angular momentum flux (AMF) $F_H(x)$ — the amount of angular momentum carried by the wake, which can be written as (RP12)

$$F_H(x) = \int_0^{\infty} F_{H,k_y}(x) dk_y, \quad (29)$$

$$F_{H,k_y} = 4\pi \Sigma_0(x) [\Re(v)\Re(u) + \Im(v)\Im(u)],$$

where F_{H,k_y} is the angular momentum flux carried by a particular azimuthal mode of the wave. Angular mo-

mentum conservation demands the radial divergence of the AMF $dF_{H,k_y}/dx$ to be equal to $(dT/dx)_{k_y}$. RP12 have demonstrated this to be the case for a uniform disk and their calculation can be trivially extended for an arbitrary non-uniform disk density profile. This is done (separately for each azimuthal mode) by writing F_{H,k_y} in terms of v using (21), differentiating with respect to x , and then rearranging the terms proportional to $v\partial v/\partial x$ with the aid of equation (18). As a result one indeed finds that $dF_{H,k_y}/dx = (dT/dx)_{k_y}$.

4.1. Lindblad Resonance torque prescription

To derive the asymptotic torque density behavior (4) in physical space GT80 have explicitly assumed that the angular momentum associated with a particular low-order ($k_y h \lesssim 1$) harmonic of the perturbing potential gets added to the density wave exactly at the Lindblad resonance corresponding to that mode, i.e. $x_L(k_y) = 2/(3k_y)$. Dong et al. (2011a) have extended this assumption to modes with arbitrary values of k_y to obtain a so-called *Lindblad Resonance* (LR) prescription for the angular momentum flux $F_H^{\text{LR}}(x)$, which they used as a benchmark for comparing with their numerical results for uniform disks. This prescription is given by the following formula (Dong et al. 2011a):

$$F_H^{\text{LR}}(x) = \frac{1}{h} \int_{\mu_{\min}(x)}^{\infty} d\mu \frac{F_H(\mu)}{F_H^{\text{WKB}}(\mu)} F_H^{\text{WKB}}(\mu), \quad (30)$$

$$F_H^{\text{WKB}}(\mu) = \frac{4}{3} \Sigma_\infty \mu^2 \left(\frac{GM_p}{c_s} \right)^2 \times [2K_0(2/3) + K_1(2/3)]^2, \quad (31)$$

where $F_H(\mu)/F_H^{\text{WKB}}(\mu)$ is the ratio of the actual AMF contribution carried by a particular harmonic with $\mu \equiv k_y h$ far from the perturber to the value of the same quantity obtained using WKB approximation. This ratio has been computed numerically by GT80 for arbitrary μ ; in the limit $\mu \rightarrow 0$ it tends to unity.

In equation (30) $\mu_{\min}(x) = (2/3)h/x$ is the minimum value of $k_y h$ for which the position of a corresponding Lindblad resonance (in a uniform disk) satisfies $x_L(k_y) < x$. Thus $F_H^{\text{LR}}(x)$ represents the sum of the AMFs (measured at $x \rightarrow \infty$) carried by all individual Fourier modes having their Lindblad resonances lying at $x_L(k_y) < x$. Note that in computing $\mu_{\min}(x)$ we do not use the positions of Lindblad resonances accounting for disk nonuniformity (Equation 24) — we found this prescription for $x_L(k_y)$ to provide F_H^{LR} inconsistent with numerical results, see §6.1.

The prescription (30) is formulated for a disk with constant density Σ_∞ . We extend it to disks with gaps by first defining a *Lindblad resonance torque density* in a uniform disk as $dT^{\text{LR}}(x)/dx|_u \equiv dF_H^{\text{LR}}(x)/dx$, and then using this torque density in equation (3):

$$\frac{dT^{\text{LR}}(x)}{dx} = \frac{\Sigma_0(x)}{\Sigma_\infty} \cdot \frac{dF_H^{\text{LR}}(x)}{dx}. \quad (32)$$

Note that for $|x| \gtrsim h$ one has $\mu_{\min} \lesssim 1$ and $dT^{\text{LR}}(x)/dx|_u$ reduces to the standard GT80 expression (4). Most studies of tidal coupling in non-uniform disks have used this asymptotic form of the prescription (32), i.e. equation (3) with $dT/dr|_u$ given by equation (4), to characterize the torque density; use of equation (30) simply allows us to extend this prescription to arbitrary values of x .

The prescription (30) is equivalent to assuming that each potential harmonic exerts torque only in the immediate vicinity of its Lindblad resonance, a notion that has been shown by RP12 to be incorrect in the shearing sheet approximation even for $\mu \lesssim 1$. In reality Lindblad resonances have finite width, which leads to the nontrivial interference between them, resulting in the negative torque density phenomenon at $|x| \gtrsim 3.2h$ (Dong et al. 2011a; RP12) not captured by the GT80 analysis. Despite this failure of the assumed discreteness of the Lindblad resonance, we still use $F_H^{\text{LR}}(x)$ in this work to compare with our new results as it provides an interesting reference point.

5. TORQUE BEHAVIOR IN FOURIER SPACE

We start our investigation of the angular momentum exchange between the disk and the perturber by exploring the torque behavior for individual Fourier harmonics. We explore both the spatial structure of the torque density due to individual modes (§5.1), as well as their contribution to the full torque far from the perturber (§5.2).

5.1. Spatial structure of $(dT/dx)_{k_y}$

In Figure 4 we show the torque density for individual Fourier harmonics $(dT/dx)_{k_y}(x)$ computed using equation (28), at different radial separations x . These calculations assume our fiducial density profile (23) with parameters $\delta = 5h$, $\Sigma_{\min} = 3 \times 10^{-4}$, and $n = 2$. We show both the torque density per unit local surface density (i.e. $(dT/dx)_{k_y}(x)$ normalized by $\Sigma_0(x)$; left panels) as well as the pure $(dT/dx)_{k_y}(x)$ (divided by constant Σ_∞ , right panels). We also display $(dT/dx)_{k_y}|_u$ computed for a uniform disk (see Figure 3 of RP12), normalizing it by Σ_∞ in the left panels (which yields the torque density per unit local surface density in a homogeneous disk) and also multiplying by $\Sigma_0(x)/\Sigma_\infty^2$ (to incorporate the local density correction) in the right panels. In all cases torque density is properly normalized to make it dimensionless. In the left panels of this Figure we indicate the position of the Lindblad resonances with arrows, both for an inhomogeneous (see equation [24]) and a uniform disks.

In panels (a) and (b), we plot $(dT/dx)_{k_y}(x)$ for $k_y h = 1$. The corresponding Lindblad resonance lies at $x/h = 2/3$, in the flat bottom of the gap and is thus the same for both uniform and fully non-uniform disks. Moreover, the waveform inside the gap perfectly matches that of the uniform disk since the profile has constant density there. Note that the torque density is not sharply localized at the Lindblad resonance position $x_L(k_y)$ but is extended over a reasonably broad radial range around x_L , with quite pronounced (even though damped) oscillations of $(dT/dx)_{k_y}(x)$ clearly visible even for $x \gg x_L$. This additionally confirms the finite and non-negligible width of resonances previously pointed out by Artymowicz (1993) and RP12.

At $x > 4h$, where Σ_0 starts to increase, we observe that the torque density decreases its amplitude quite abruptly compared to the uniform disk calculation, see panel (b). By looking at the shaded regions one can notice that the two calculations start differing at $\Sigma_0 \sim 10^{-3}\Sigma_\infty$ where the density gradients become significant. This damping of the amplitude compared to the homogeneous disk case is the consequence of incorporating the disk non-uniformity in the fluid equations, also clearly visible for other values of $k_y h$ at the gap edge (see below).

In panels (c) and (d) we show the torque density for $k_y h = 0.32$ mode, for which there are multiple Lindblad resonances at $x/h = 2.1, 3.8, \text{ and } 4.5$, see Figure 2 (the uniform disk has, of course, just a single one at $x/h = 2/(3k_y h) \approx 2.1$). These are indicated with arrows in panel (c) and it can be seen from both panels that the extra resonances located at $x \sim 4h$ give rise to positive torque density contribution and overall significant phase shift compared to the uniform disk case. Also, the amplitude of the torque density oscillations far from the resonances is greatly reduced in the self-consistent calculation of $(dT/dx)_{k_y}(x)$ so that in panel (d) we even multiply the uniform disk curve by 0.05 for it to have an amplitude comparable to that of the fully non-uniform disk calculation.

The mode with $k_y h \approx 0.14$ shown in Figure 4e,f has a single Lindblad resonance at $x_L \approx 5h$, which coincides with the resonance position in a uniform disk (see Figure 2). Despite this coincidence the waveforms for the uniform and non-uniform disk calculations are very different

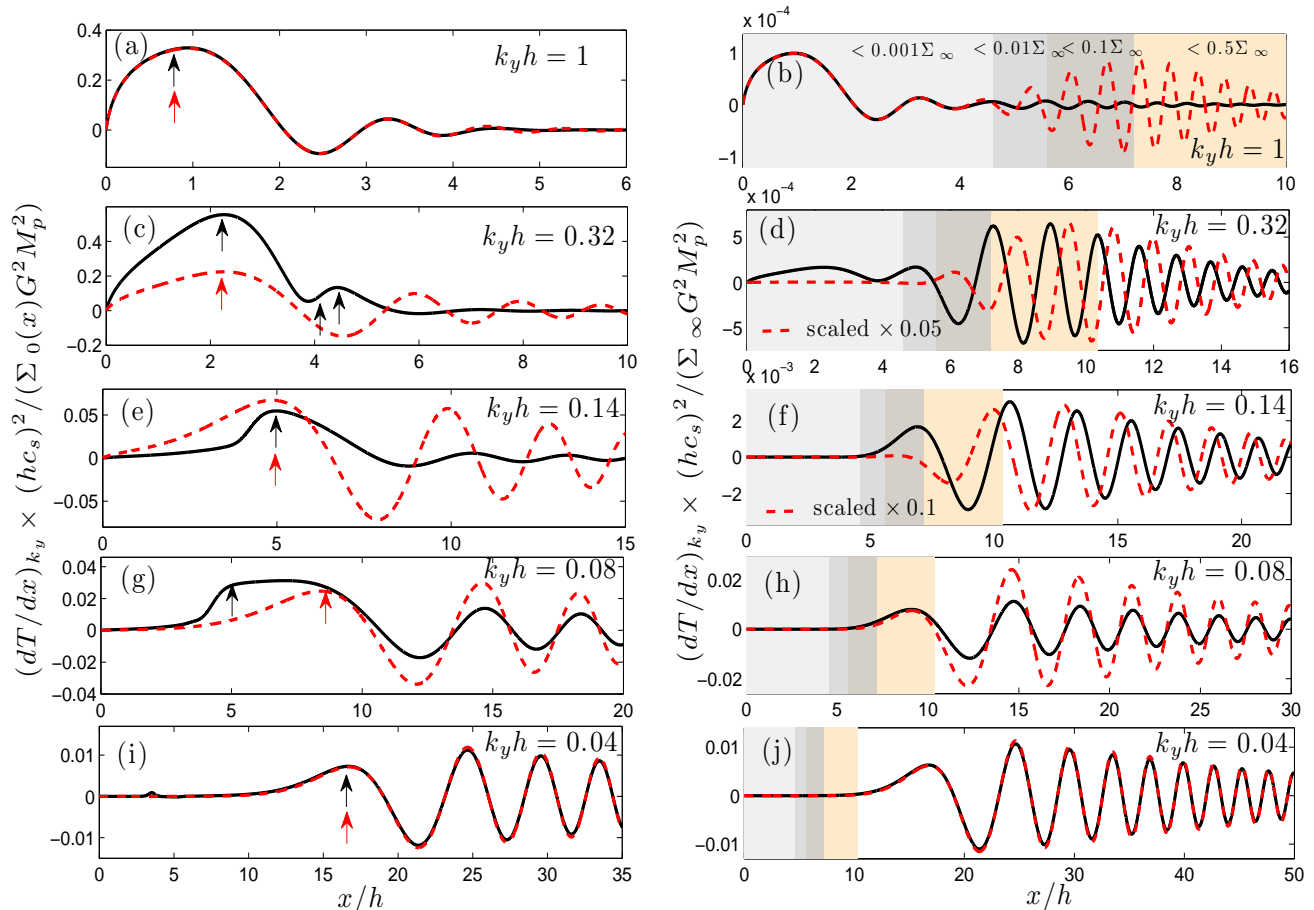


FIG. 4.— *Left panels*: torque density per unit surface density $\Sigma_0(x)$ for the non-uniform disk (black solid lines) and per Σ_∞ for the uniform density case (red dashed lines) produced by modes of a given k_y . *Right panels*: same curves but multiplied by the non-uniform density profile $\Sigma(x)/\Sigma_\infty$ (i.e. black solid lines now show pure non-uniform disk torque density $(dT/dx)_{k_y}$). Gap model given by Eq. (23) with parameters $\delta = 5h$, $\Sigma_{\min} = 3 \times 10^{-4}$, and $n = 2$. Black and red arrows in the left panel indicate the position of the Lindblad resonances in non-uniform and uniform disks, respectively. In panels (d) and (f) we scale the results for the uniform case by 0.05 and 0.1, respectively, to facilitate comparison. Shaded regions in right panels indicate (from left to right) the regions where $\Sigma_0(x)$ is less than $0.001 \times \Sigma_\infty$, $0.01 \times \Sigma_\infty$, $0.1 \times \Sigma_\infty$, and $0.5 \times \Sigma_\infty$.

from each other both in terms of shape and the overall amplitude (note that the uniform disk curve in panel (f) has been multiplied by 0.1).

The mode with $k_y h = 0.08$ shown in Figure 4g,h has its (single) Lindblad resonance at $x \approx 5.1h$, considerably shifted inward from the corresponding uniform disk resonance position at $x = 8.3h$. The torque density normalized by $\Sigma_0(x)$ (see panel (g)) has a rather broad spatial distribution extending from $x \sim 5h$ so $x \sim 8h$ before starting to oscillate at an amplitude reduced roughly by a factor of 2 compared to the uniform disk calculation.

Finally, in panels (i) and (j) we show the mode $k_y h = 0.04$ for which $x_L \approx 16h$ lies where the density gradients are negligible. As a result, calculations in a uniform and nonuniform disk cases perfectly coincide, demonstrating that far from gap torque excitation is well described by the uniform disk theory of RP12.

To summarize, the spatial distribution of the torque density for individual Fourier harmonics can be substantially modified in non-uniform disks in regions where the density gradients are large, compared to the case of a constant density disk. The differences arise both because of the displacement of the Lindblad resonances and be-

cause of the different mathematical structure of the fluid equations in the non-uniform disk case.

5.2. Angular momentum flux in Fourier space

We now study the behavior of the AMF as a function of k_y for $x \rightarrow \infty$. Since, as mentioned in §4, $F_{H,k_y}(x)$ is identical (up to a constant offset) to the integrated torque we look at the behavior of

$$T(k_y) = \int_0^\infty \left(\frac{dT}{dx} \right)_{k_y} dx \quad (33)$$

in Fourier space, where $(dT/dx)_{k_y}$ is given by our numerical calculations.

As a point of comparison we also use the variation of $F_H(k_y) \equiv F_{H,k_y}(x \rightarrow \infty)$ with k_y in a homogeneous disk (previously computed by GT80) which we additionally multiply by $\Sigma_0(x_L(k_y))$ to account for the disk non-uniformity (where we take $x_L(k_y) = 2/(3k_y)$). This re-scaling implies that each mode carries the AMF from a uniform disk corrected by the local density at the position where the excitation of this mode occurs in a uni-

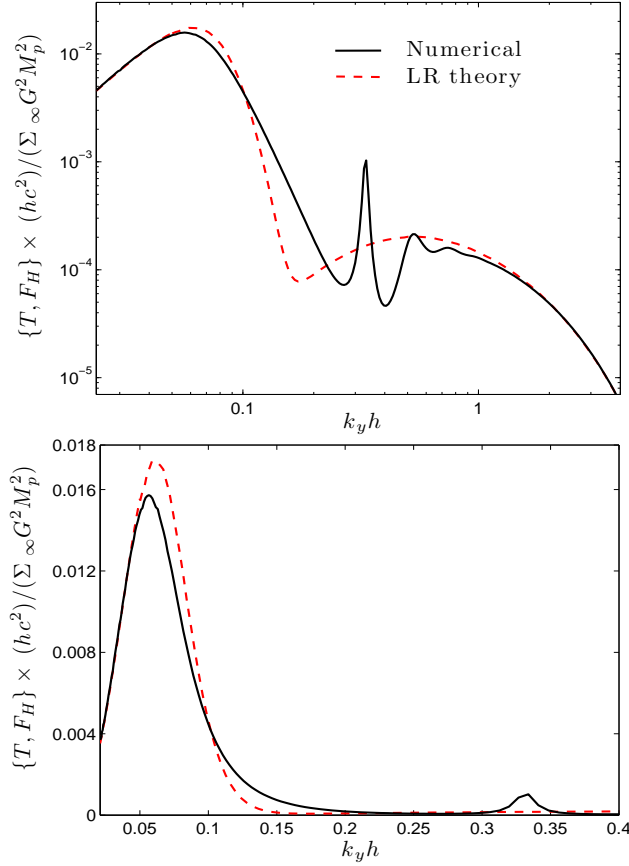


FIG. 5.— Angular momentum flux (or integrated torque) far from the planet ($x \rightarrow \infty$) in Fourier space (logarithmic coordinates at the top, linear at the bottom) for a gap model given by Eq. (23) with $\delta = 5h$, $\Sigma_{\min} = 3 \times 10^{-4}$, and $n = 2$. The black solid line indicates the results from equation (33) and the red dashed line results from the LR theory described in §5.2.

form disk. This procedure is a version of the LR theory described in §4.1 in Fourier space, as it incorporates the two major ingredients from that prescription: the localized mode excitations at a Lindblad resonance and the AMF computed for a uniform density disk.

In Figure 5, we plot the torque from our calculations and the AMF from the LR theory for our fiducial model with $\delta = 5h$, $\Sigma_{\min} = 3 \times 10^{-4}$, and $n = 2$. The first thing we notice is that both expressions coincide in the limits of long wavelengths $k_y h < 0.05$ and short wavelengths $k_y h > 2$. This is expected to happen since in both limits the satellite excites waves in the flat parts of the disk — far outside the gap for $k_y h < 0.05$ and deep inside the gap, in the flat part of the density profile for $k_y h > 2$. For that reason the positions of the resonances and the waveforms coincide in our non-uniform calculation and in a uniform disk. But in the intermediate range of k_y there are appreciable differences between the LR theory and our calculations, mainly due to effect of the shifted Lindblad resonances as we discuss next.

First, for $k_y h \sim 0.05 - 0.1$ Figure 2 demonstrates that Lindblad resonances are shifted towards the perturber and the excitation occurs in *lower* density region of the disk compared to the case when resonances lie at $x = 2/(3k_y)$ (as appropriate for homogeneous disk). Because

of this reduction of the background surface density the torque produced by modes in this range of k_y ends up being lower than the AMF computed according to the LR theory (which assumes $x_L = 2/(3k_y)$), even though the coupling to the perturbation potential is stronger at smaller $|x|$. Conversely, modes with $k_y h \sim 0.1 - 0.2$ have their resonances shifted *outwards*, into the higher density part of the gap profile, which explains their higher values of $T(k_y)$ compared to the LR theory AMF.

At higher values of k_y there is a point where resonances split and take place at multiple locations, as discussed in §2.3. According to Figure 2 this is the case for $k_y h \gtrsim 0.2$, which explains the intricate shape of $T(k_y)$ for these modes — a peak at $k_y h = 0.2 - 0.3$ where the Lindblad resonances are split in three (see Figure 4c,d for illustration of the torque density behavior for these modes). The innermost resonance almost coincides with that in a uniform disk, but the other two are located further out, in a higher density region of the gap, explaining the spike of $T(k_y)$ for these values of k_y .

Complicated structure of the $T(k_y)$ curve around the peak at $k_y h \sim 0.32$ does not have a straightforward explanation and is probably related to the intricate behavior of the torque density when the excitation is taking place at multiple locations at the gap edge.

6. TORQUE BEHAVIOR IN PHYSICAL SPACE

We now explore the behavior of the torque integrated over all Fourier modes in physical space. We look at the spatial distribution of the torque density in §6.1 and of the integrated torque $T(x)$ in §6.2.

6.1. Torque density

In the top panel of Figure 6, we plot the torque density dT/dx (integrated over all k_y , see equation [28]) per unit of the local surface density $\Sigma_0(x)$ for our fiducial model and make a comparison with the LR theory behavior given by equation (32). In the lower panel of Figure 6 we directly compare dT/dx and dT^{LR}/dx . One can clearly see a significant discrepancy between the two.

The disagreement at $|x| \lesssim 5h$, where the surface density is close to constant (the bottom part of the gap) is expected based on the RP12 results — one can see that our dT/dx is negative for $x \sim (3 - 4)h$ which is just the manifestation of the negative torque density phenomenon (Dong et al. 2011a) not captured by the dT^{LR}/dx . Also, the overall shape of dT/dx and dT^{LR}/dx is different for $|x| \lesssim 3h$ — again well known from the uniform disk studies of Dong et al. (2011a) and RP12.

The discrepancies at $|x| \gtrsim 5h$ where the density gradients are important can only be understood by fully accounting for the disk non-uniformity. According to GT80 for $|x| \gtrsim h$ the LR theory predicts $\Sigma_0^{-1} dT/dx \approx 2.5(h/x)^4$ (in this section we refer to the torque density in units of $\Sigma_\infty G^2 M_p^2 / (hc_s)^2$), see equation (4) and §4.1. However, our self-consistent nonuniform disk calculations suggest that the torque density decays *exponentially* $\propto \exp(-0.8x/h)$ for $|x| \gtrsim 5h$, as shown in the upper panel of Figure 6. This result casts serious doubt on all torque prescriptions used in the literature that adopt the GT80 functional form to account for the tidal torque. The exponential fall-off is clearly related to the presence of strong density gradients at the gap edge but

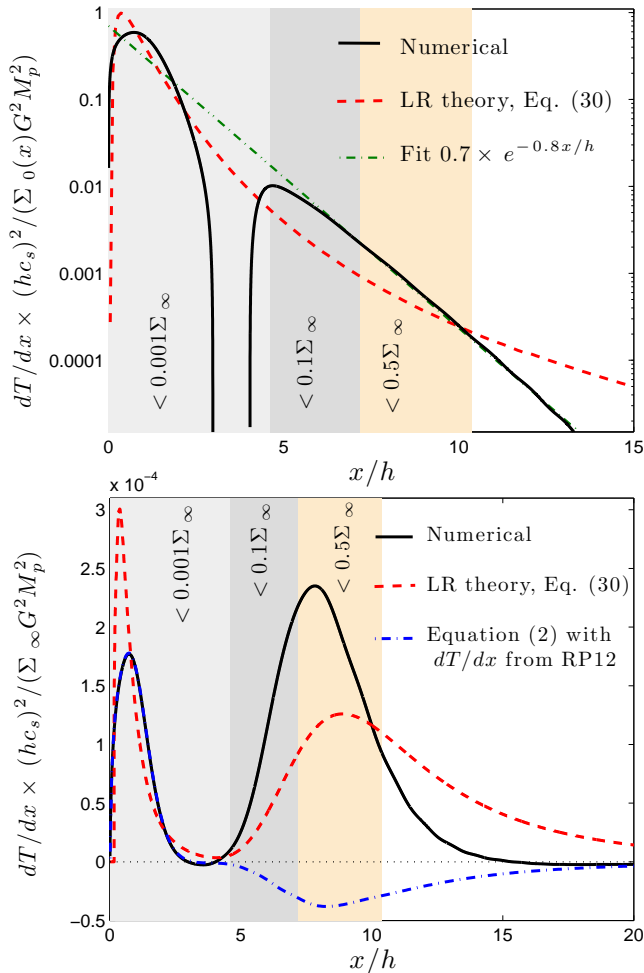


FIG. 6.— Torque density dT/dx obtained self-consistently for a non-uniform disk using our numerical results (solid black lines) and that from the LR prescription (§4.1; dashed red lines) for a gap model given by Eq. (23) with parameters $\delta = 5h$, $\Sigma_{\min} = 3 \times 10^{-4}$, and $n = 2$. In the *upper panel* we normalize by the surface density $\Sigma_0(x)$ and add a numerical fit to show the *exponential* fall-off of dT/dx outside the gap. In the *lower panel* we normalize by the density at infinity Σ_∞ and also display dT/dx computed using the prescription in Eq. (3) with the uniform disk torque density properly accounting for the negative excitation torque density phenomenon (RP12). The latter curve demonstrates the conceptual failure of a simple prescription (3).

we could not find a simple qualitative explanation for this particular form of the torque decay. We just note here that this behavior of dT/dx has nothing to do with the presence of the exponential term in equation (23), which is introduced only to guarantee the flat density profile in the bottom part of the gap. We provide more details on the exponential decay of dT/dx in Appendix B.

Apart from the discrepancy in the functional form, the self-consistent specific torque density is also more concentrated towards the perturber at the gap edge, and has a larger amplitude there. This effect can be understood from our previous analysis of the shifted Lindblad resonances that tend to accumulate at the gap edge (see Figures 2 and 4), increasing excitation torque density in this region and reducing it outside of it, at $|x| \gtrsim 10h$. This effect has not been taken into account in previous studies but it does drastically change the overall shape of the torque density.

We tried to improve the performance of the LR theory (§4.1) by assigning torque contributions of individual modes not to $x_L = 2/(3k_y)$ (which is appropriate only for a uniform disk), but to $x_L(k_y)$ given by the self-consistent calculation in a non-uniform disk, see equation (24). Unfortunately, the agreement with our fully self-consistent calculation has gotten even worse (for this reason we did not pursue this idea further), which suggests that properly accounting for the resonance overlap is also very important for getting the correct spatial distribution of the torque.

Far enough from the gap edge, where $\Sigma_0(x)$ flattens out, the excitation torque density becomes negative, which is a direct manifestation of the negative torque density phenomenon (Dong et al. 2011a). For the adopted gap profile this happens at $x \approx 15h$, and dT/dx stays negative out to infinity and agrees with the asymptotic behavior $-0.63(h/x)^4$ derived in RP12.

Additionally, in the bottom panel of Figure 6 (dot-dashed curve) we plot dT/dx calculated according to the simplified prescription (3) but using the correct excitation torque density for the uniform disk $dT/dx|_u$ calculated in RP12 instead of the GT80 prescription (4). One can see that this calculation fails miserably compared to the correct dT/dx : it predicts negative excitation torque density for $x > 3.2h$, which is the direct consequence of the negative torque density phenomenon in the uniform disks. Because of this, as we will later see in Figure 7, the use of this prescription results in the *negative* integrated torque deposited in the density wave by the perturber, which cannot be true in a real disk.

The point of this last exercise was to illustrate the failure of the simple prescription (3), which yields unphysical results even when it uses physically motivated ingredients — the spatial behavior of $dT/dx|_u$ derived in RP12 as opposed to the asymptotic formula (4).

6.2. Integrated torque and AMF

In Figure 7, we plot the integrated torque $T(x)$ for our fiducial model as well as the AMF $F_H(x)$ calculated using equation (29). The two have small relative vertical offset but are otherwise identical, as expected from the discussion in §4. We also display $T^{\text{LR}}(x)$ obtained by integrating dT^{LR}/dx given by equation (32) from zero to x .

All these expressions almost coincide within the gap. This happens because in the flat-bottomed gap different methods of computing integrated torque should yield the same result: a total torque (or AMF) of ≈ 0.93 (GT80) in units of the plot times $\Sigma_{\min} = 3 \times 10^{-4}$. This equivalence of the full torque calculations in the Fourier space ($T^{\text{LR}}(x)$) and physical space ($T(x)$) has been previously mentioned in RP12.

At the gap edge, for $|x| \gtrsim 5h$, one finds that $T(x)$ increases faster than $T^{\text{LR}}(x)$, which is a direct consequence of the torque density dT/dx in a self-consistent non-uniform disk calculation being rather concentrated towards the perturber, see §6.1. Quite remarkably, despite this difference at the gap edge the accumulated torque at infinity nearly coincides with that given by the simple theoretical prescription $T^{\text{LR}}(x)$: our self-consistent calculation yields full torque $\approx 1.2 \times 10^{-3}$, while the LR theory predicts $\approx 1.3 \times 10^{-3}$ (see Figure 7 at $x = 30h$ for

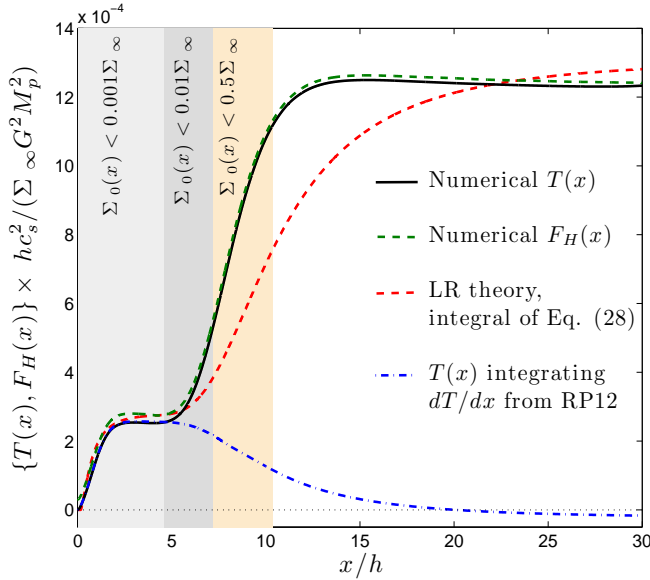


FIG. 7.— Integrated torque $T(x)$ from our numerical results (solid black line), the LR theory (dashed red line), and the integration of the torque density from uniform density disk (RP12) using the prescription (3) (dot-dashed blue line). Dashed green line displays the AMF $F_H(x)$ obtained from Equation (29) and, as expected, agrees with $T(x)$. Note that the RP12 prescription for $dT/dx|_u$ used in combination with equation (3) results in *negative* integrated torque as $x \rightarrow \infty$, which is unphysical (see §6.1 for details). Results are for a gap model (23) with $\delta = 5h$, $\Sigma_{\min} = 3 \times 10^{-4}$, and $n = 2$.

reference). This means that the *total* torque exerted on the disk (but not the spatial distribution of the torque density!) is well described by the simple theoretical prescription (essentially $T^{\text{LR}}(x)$ based on asymptotic scaling [4]) that has been broadly used in the literature.

We do not have a fully satisfactory explanation for this coincidence except for the following observation. In the lower panel of Figure 5 we display the torque in Fourier space (on linear scale) for $k_y h < 0.4$. There it can be seen that our non-uniform disk calculation generate almost the same amount of torque as the theoretical prescription (integrals under the curves are roughly the same), meaning that the torque deficit with respect to the LR theory visible for $k_y h \lesssim 0.1$ is almost exactly compensated by the torque excess for $k_y h \gtrsim 0.1$. This means that the effect of resonances, which are being shifted to lower density regions resulting in lower torque contribution (smaller $k_y h$) is closely counterbalanced by the torque enhancement due to the resonances displaced to higher density region (larger $k_y h$). This is an interesting result, which only weakly depends on the exact gap profile as we empirically show next.

7. EFFECT OF VARYING GAP SHAPE PARAMETERS

So far, we showed the results obtained for a specific gap density profile given by equation (23) with a certain set of parameters, namely $\delta = 5h$, $\Sigma_{\min} = 3 \times 10^{-4}$, and $n = 2$. It would of course be much better to discuss torque structure not for an arbitrary model of the gap profile but for the one which is realized in nature. However, the calculation of such profile must self-consistently couple the calculation of the torque excitation (such as the one done here) with the description of the wave damping, and this is beyond the scope of this work. However, we can

still explore the general *trends* in the torque behavior as the various properties of the gap (its depth, width, etc.) are varied. This is what we do now.

7.1. Steepness of the gap edge (variation of n)

As discussed in §2.2 and shown in Figure 1, the parameter n controls the steepness of the density gradients at the gap edge. In panels (a) and (d) of Figure 8 we plot the excitation torque density and the integrated torque, respectively, for $n = 2, 4, 6$, while fixing $\delta = 5h$ and $\Sigma_{\min} = 3 \times 10^{-4}$.

As n is increased the gradients become larger and, therefore, the amplitude of the variation of κ^2 around the gap edge becomes larger. This leads to higher resonance accumulation closer to the perturber, and Σ_0 gets higher there as well. As a result, the torque density gets more concentrated towards the gap center with increasing n , see Figure 8a: for $n = 6$ almost all the torque is excited within the range $5h \lesssim x \lesssim 10h$, while for $n = 2$ this region extends out to $x \sim 15h$.

The integrated torque also increases with n since closer to the gap center excitation by the perturber is more effective, depositing more angular momentum into the density waves. We see from Figure 8d that the density profile with $n = 2$ results in a total torque of $\sim 1.2 \times 10^{-3}$ in units of $(GM_p)^2 \Sigma_\infty / hc_s^2$, while using $n = 6$ we obtain $\sim 2.1 \times 10^{-3}$.

This Figure also demonstrates that for all values of n the LR theory predicts more extended torque density distribution than we find in self-consistent calculations, see §6.1. Nevertheless, the integrated torque at $|x| \rightarrow \infty$ is still well predicted by the LR theory, the point we previously made in §6.2. The largest relative difference of $\sim 13\%$ is found for $n = 6$, for which we obtain the integrated torque of $\sim 2.1 \times 10^{-3}$, while the LR prescription gives $\sim 2.4 \times 10^{-3}$.

7.2. Width of the gap (variation of δ)

In Figure 8b,e we vary the width of the gap by slightly changing δ , but fixing $\Sigma_{\min} = 3 \times 10^{-4}$ and $n = 2$. As expected, for narrower gaps the torque density peaks closer to the planet and the integrated torque reaches higher values, simply because the strength of the tidal coupling is higher closer to the perturber.

Figure 8e shows that the integrated torque predicted by the LR theory tends to better match the self-consistent calculation as the gap width is increased. Also, the dependence of the $T(x \rightarrow \infty)$ on δ is not linear: decreasing δ from $6h$ to $5.5h$ results in $\sim 14\%$ increase of the integrated torque, while going from $5.5h$ to $5h$ results in the increase of $\sim 25\%$. Using the fact that the LR theory gives a reasonably good approximation to the integrated torque behavior, and adopting the prescription (3) with $dT/dr|_u$ given by equation (4) one can estimate that the total torque excited outside the density gap scales as $T(x > \delta) \propto (\delta/h)^3$. We verified this simple scaling by calculating integrated torque for density profiles with $\delta = (4 - 8)h$. This behavior is in agreement with Papaloizou & Lin (1984) who present the same scaling for the one-sided torque.

7.3. Gap depth (variation of Σ_{\min})

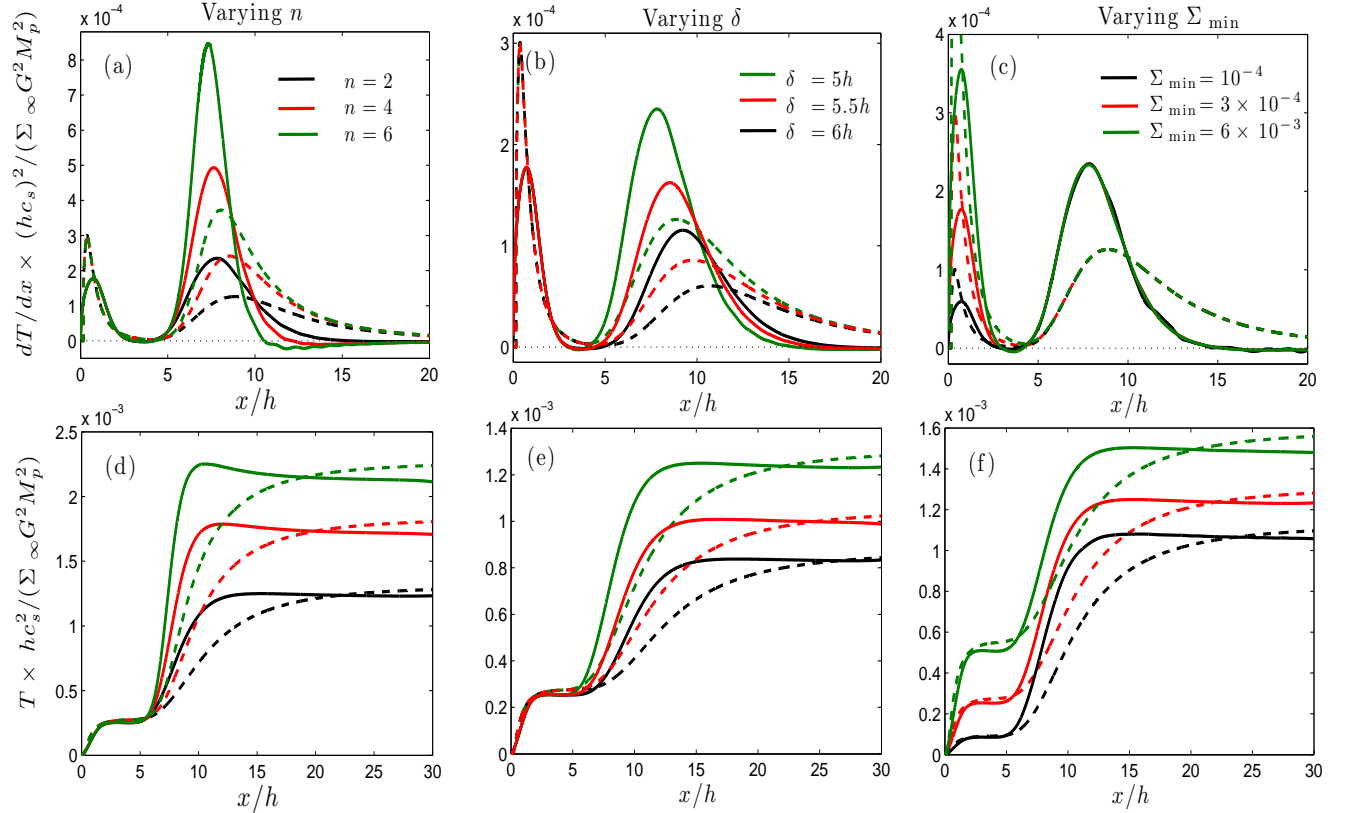


FIG. 8.— Torque density (upper panels a, c, and e) and integrated torque (lower panels b, d, and f) for a gap model given by Eq. (23) varying the three parameters n , δ , and Σ_{\min} one at a time with respect to our fiducial choice $\delta = 5h$, $\Sigma_{\min} = 3 \times 10^{-4}$, and $n = 2$. In panel (a) and (d) we vary n , fixing δ , Σ_{\min} , in panel (b) and (e) we vary δ , and in panel (c) and (f) we vary Σ_{\min} . Dashed line indicates the results from the LR theory (§4.1).

In Figure 8c,f we vary the dimensionless gap depth Σ_{\min} from 10^{-4} to 10^{-3} , while fixing $n = 2$ and $\delta = 5h$. One can see that changing Σ_{\min} only affects the torque density and the full torque accumulated inside the gap (in a linear fashion); outside the gap (for $x > 4h$) torque structure remains unchanged.

As Σ_{\min} is increased there is a point at which the integrated torque starts being dominated by the excitation inside the gap, in the immediate vicinity of the perturber. One can easily predict when this happens. For a flat-bottomed gap profile like the one we consider in this work the torque accumulated inside the gap is $T(x < \delta) \sim 0.9 \Sigma_{\min} \Sigma_{\infty} G^2 M_p^2 / hc_s^2$ (RP12 and GT80) if the gap width δ is larger than about $2h$ — the extent or the region where most of the torque excitation occurs in a uniform disk. This exceeds the torque $T(x > \delta)$ excited outside the gap for

$$\Sigma_{\min} \gtrsim \frac{T(x > \delta) hc_s^2}{0.9 \Sigma_{\infty} G^2 M_p^2} \approx 2.8 h^3 \int_{\delta}^{\infty} \frac{\Sigma_0(x)}{x^4} dx, \quad (34)$$

since the value of $T(x > \delta)$ is well approximated by the LR theory using the prescription (3) with $dT/dr|_u$ given by equation (4). In the case shown in Figure 8c,f the critical value of Σ_{\min} is $\approx 10^{-2}$, i.e. the integrated torque in this case is dominated by the excitation at the edge of

the disk only when the density inside the gap is depleted below 1% of Σ_{∞} .

Finally, after trying different combination of parameters for the density profile, we observe that the torque density always decays *exponentially* outside the gap in regions where the density gradients are important, as discussed in §6.1. In Appendix B we construct an empirical fit for the torque density in this region represented by equation (B1).

8. DISCUSSION

The main result of this work is a new, self-consistent calculation of the torque excitation by a massive perturber in a non-uniform disk. We clearly show that the existing torque density prescriptions (Lin & Papaloizou 1986; Trilling et al. 1998; Armitage & Natarajan 2002; Armitage et al. 2002), majority of which are based on the GT80 asymptotic result (4), provide inadequate description of the spatial distribution of dT/dr in disks with gaps.

In particular, we find that for deep gaps the torque excitation is more concentrated towards the perturber than the standard prescription (3) with $dT/dr|_u$ from equation (4) would predict. Also, in regions where density gradients are non-zero we find the fall-off of the torque density to be *exponential* as opposed to the x^{-4} dependence that is assumed in all previous works (see

Goldreich & Tremaine (1980); Lin & Papaloizou (1979); Papaloizou & Lin (1984); Lin & Papaloizou (1986) and references therein). Moreover, far from the gap edge, where the density flattens out, we recover the negative torque density phenomenon previously found by Dong et al. (2011a) and RP12 in a uniform disk.

There are three main reasons for these differences:

1. Lindblad resonances in non-uniform disks are shifted with respect to their constant density disk analogues, and often occur at multiple locations (§2.3).
2. Spatial behavior of the eigenmodes of the perturbed fluid variables is different in a non-uniform disk (§5.1).
3. Interference of different Lindblad resonances important for both uniform and non-uniform disks is usually not accounted for by the LR-type prescriptions (§4.1).

One can try to improve the existing semi-analytical torque prescriptions. Previously there have been some attempts to incorporate the (weak) disk non-uniformity in the LR prescription for dT/dr by accounting for only the resonance shift (Menou & Goodman 2004; Ward 1997; Matsumura et al. 2007). We checked the performance of this procedure in §6.1 but found that it does not improve (at least for strong density variations) the agreement with the self-consistent calculation. And the other two issues listed above are clearly very difficult to account for in any simple way.

Unfortunately, an accurate calculation of dT/dr for an arbitrary $\Sigma_0(r)$ profile, which is necessary for studies of the coupled evolution of the perturber and the surrounding disk (Lin & Papaloizou 1986; Trilling et al. 1998; Ivanov et al. 1999; Armitage et al. 2002; Chang et al. 2010), is rather computationally-intensive as outlined in §3.1. In this regard it would be nice to have a simple analytical fit to the actual excitation torque density behavior and in Appendix B we provide a simple one-parameter formula (B1) for dT/dr for exactly this purpose. Even though there is some ambiguity in choosing the proper fit (it depends on a single parameter α , which is somewhat different for different gap profiles) this approach provides a basis for finding better semi-analytical representations of the dT/dr behavior useful for long-term numerical calculations of the disk-satellite interaction.

Despite the different predictions for the torque density dT/dr we found that the LR theory outlined in §2.3 does produce a reasonable description of the *total integrated* torque, within $\sim 20\%$ of that found in a self-consistent calculation for different values of the gap density profile, see §7. Previously Papaloizou & Lin (1984) carried out a numerical torque calculation for a polytropic disk truncated by a massive perturber located at the distance δ from the disk edge, and found that the integrated torque scales as $\sim \delta^{-3}$. This is in agreement with our results described in §7.2 and supports the observation that the LR theory provides reasonably accurate description of the full one-sided torque exerted on the disk.

Based on this remarkable result one may decide that the orbital evolution of the perturber should be insensitive to the discrepancy in the torque density calculation described above, simply because the variation of the

perturber's angular momentum depends on the full integrated torque it exerts on the disk. This, however, is not true since the integrated torque does sensitively depend on the gap density profile (see §7), and the latter is a function of the torque density distribution in the disk. Thus, dT/dr is in fact involved (even though indirectly) in determining the rate of migration of the perturber. This makes any statements regarding the Type II migration speed in protoplanetary disks and the rate of SMBH inspiral due to interaction with the circumbinary disk dependent on our understanding of the torque density in non-uniform disks, which our work aims to provide.

8.1. Nonlinearity of the density wave

We noticed in §3.2 that the conservation of the angular momentum forces the relative amplitude of the density wake Σ_1/Σ_0 to *decrease* as the wave climbs up the density gradient at the gap edge. Interestingly, even though the normalized Σ_1/Σ_0 does not vary much as the wave travels through the gap edge, the angular momentum density varies a lot; this is because the latter is sensitive to the overall wake *shape* and not just its amplitude.

The variation of the relative density perturbation has interesting implications for the strength of the density waves outside the gap. In particular, from the fact that the normalized wake amplitude in Figure 3 does not vary much with x it follows that the wave nonlinearity measured by the ratio $\Sigma_1/\Sigma_0 \propto (x/\Sigma_0(x))^{1/2}$ should decrease by a factor of $\sim [(\delta/h)/\Sigma_{\min}]^{1/2}$ between the bottom of the gap and the part of the disk just outside of the gap, where $\Sigma_0 \sim \Sigma_\infty$. For clean gaps with small Σ_{\min} this factor can be quite significant, ≈ 0.2 for a gap with the width of $\delta = 5h$ and density contrast at the bottom $\Sigma_{\min} = 10^{-2}$ (this factor is ~ 0.05 for the situation shown in Figure 3c). Thus, even if the density wave starts out highly nonlinear ($\Sigma_1/\Sigma_0 \gtrsim 1$) inside the gap near the planet, it may become linear upon propagating out of the gap. The initial wave nonlinearity in the flat part of the density profile near the planet is $\Sigma_1/\Sigma_0 \sim M_p/M_{\text{th}}$, where $M_{\text{th}} \equiv c_s^3/(\Omega G)$ is the characteristic planetary mass at which the Hill radius becomes comparable to the disk scale height. This mass is about $10M_\oplus$ at 1 AU and about $60M_\oplus$ at 10 AU. Thus, a Jupiter mass planet at 10 AU would generate a highly nonlinear wave with $\Sigma_1/\Sigma_0 \sim 5$ at the bottom of the gap but the nonlinearity should drop to $\Sigma_1/\Sigma_0 \sim 1$ outside the gap for $\delta = 5h$ and $\Sigma_{\min} = 10^{-2}$, even if we neglect the wave damping (not captured by our linear theory). This demonstrates that even rather massive planets capable of opening gaps may still have their density waves in the linear regime outside the gap, depending mainly on the density contrast Σ_{\min} .

This point is rather important for the possibility of the nonlinear wave damping. Goodman & Rafikov (2001) have studied the nonlinear density wave evolution in a uniform disk and demonstrated that shock formation resulting from nonlinear effects can lead to effective damping of the wave. This study has been extended by Rafikov (2002a) to include the possibility of radial variation of Σ_0 . Our linear results suggest, in agreement with this latter work, that the nonlinear wake distortion (which ultimately results in shock formation) should slow down as the wave gets out of the gap, shock formation gets postponed and the nonlinear dissipation becomes less ef-

fective at transferring wave angular momentum to the disk material.

For massive planets the wave might shock close to the planet, while it is still propagating through the roughly uniform bottom part of the gap profile: Goodman & Rafikov (2001) estimate the shocking length of just $2h$ for a $2M_{\oplus}$ planet at 1 AU, and it is even smaller for more massive planets. Then the efficient density wave dissipation will start inside the gap but then will appreciably slow down as the wave climbs out of the gap (even though the shock will still persist). This complication should certainly affect the picture of the nonlinear wave damping and may produce important feedback for the self-consistent calculations of the gap density profile.

8.2. Astrophysical implications

Theory of disk-satellite interaction has been extensively used for understanding the interaction of protoplanetary disks with embedded planets and the evolution of SMBH binaries surrounded by circumbinary accretion disks, among other astrophysical settings. Our extensions of this theory have direct impact on our understanding of these systems.

In particular, our finding of the torque density being quite concentrated near the perturber suggests that regardless of the details of the wave damping, the angular momentum carried by the density waves should be deposited in the disk *closer to the perturber* than the conventional theory would suggest. This certainly facilitates the formation of density gaps or cavities since for the same mass of the perturber a narrower annulus of the disk needs to be cleaned by the tide. This may make Type II migration possible for lower mass planets than was previously thought.

To fully understand the impact of our results on the Type II migration and SMBH inspiral one needs to know a *self-consistent gap shape*, which can be computed only when the wave damping mechanism is specified. In this regard we note that the majority of studies of the gap or cavity opening simply ignore the issue of wave damping process and take $dT/dr|_d = dT/dr$ (Lin & Papaloizou 1986; Chang et al. 2010), i.e. assume immediate deposition of the excitation torque into the disk. However, the validity of this approximation has never been demonstrated, and calculations that do properly take wave damping into account (Ward 1997; Rafikov 2002b) result in a rather different picture of the gap opening. Our results on the wave amplitude evolution and its implications for the nonlinear wave damping in §3.2, 8.1 should be useful for understanding the spatial distribution of $dT/dr|_d$ and calculating the gap shape (and orbital evolution of the perturber) fully self-consistently.

Our present work is cast in terms of the shearing sheet approximation, which limits the direct application of its results to systems in which gaps are narrow compared to the semi-major axis of the perturber. This is the case for e.g. planets in protoplanetary disks (Lin & Papaloizou 1986; Takeuchi et al. 1996) and SMBH binaries with extreme mass ratio surrounded by an accretion disk (so-called extreme mass-ratio inspirals (EMRIs)) (Armitage & Natarajan 2002; Chang et al. 2010; Kocsis et al. 2011).

SMBHs binaries of similar mass do not fall in this category since they are known to clear out a

large and clean cavity in circumbinary gaseous disk, with inner radius comparable to the binary separation (e.g. MacFadyen & Milosavljević (2008), Cuadra et al. (2009), Shi et al. (2011), Farris et al. (2011)). However, even though the shearing sheet approximation breaks down in these systems, our results can still be used to gain qualitative insight into the dynamics of cavity clearing. In particular, concentration of the torque density towards the perturber means that cavity should be opened by lower mass ratio SMBH than was thought before.

Also, our results can help understand the excitation torque density patterns derived from simulations, most of which (MacFadyen & Milosavljević 2008; Cuadra et al. 2009; Shi et al. 2011; Farris et al. 2011; Roedig et al. 2012) agree that outside the cavity dT/dr exhibits complicated oscillatory pattern (some of these studies include additional physics such as MHD or general relativity). This behavior was not recognized before and some earlier studies (e.g. Armitage & Natarajan (2002)) tried modeling numerically derived dT/dr in the form similar to the GT80's result (4) but with the amplitude reduced by a factor of $\sim 10^{-2}$. Such low amplitude most likely results from averaging actual spatially rapidly oscillating pattern of dT/dr and then applying the $\propto |r - r_p|^{-4}$ scaling to reproduce the total integrated torque in the simulations. Clearly, usage of this prescription is likely to lead to misleading results (Liu & Shapiro 2010; Chang et al. 2010) in modeling gap shape.

MacFadyen & Milosavljević (2008) suggested that the oscillatory behavior of the torque distribution in their simulations is consistent with forcing at the 2:3 ($m = 2$) outer Lindblad resonance and tried fitting linear waveforms from Meyer-Vernet & Sicardy (1987) to spatial variation of the perturbed fluid variables. Even though they were able to reproduce qualitatively the oscillatory behavior of the numerical dT/dr the amplitude and phase of the torque density were substantially different between the numerical calculation and the analytical waveform, qualitatively consistent with the Lindblad resonance shift and reduction of perturbation amplitude in our calculations, see Figure 4f. This is certainly not surprising since not only were the Meyer-Vernet & Sicardy (1987) waveforms derived for a uniform disk, they are also valid only in the close vicinity of the Lindblad resonance. The latter limitation was removed in RP12 who came up with a fully global analytical approximation for the waveforms, but again only for a uniform disk case. Our present work is free from these constraints since it provides a way of computing $(dT/dr)_{k_y}$ for arbitrary disk surface density profile at any distance from the resonance, see §5.1. Future extensions of our approach to full cylindrical geometry will be directly applicable to the astrophysical systems such as SMBH binaries in which broad gaps or cavities are typical.

9. SUMMARY

In this work we have carried out a linear study of the tidal disk-satellite interaction in the shearing sheet approximation assuming the disk to have a non-uniform density structure to model the effect of density gaps around the perturber. The disk non-uniformity is self-consistently incorporated in the fluid equations, including the modification of the disk rotation curve due to pressure gradients, which are especially prominent at the

gap edges. This allows accurate calculation of the primary fluid variables such as the density perturbation and torque distribution in both physical and Fourier space.

Because of the rotation curve modification the Lindblad resonances get shifted towards the gap edge, often occurring at two or three locations on one side of the perturber. Because of this and the terms in fluid equations related to density gradients the waveforms of the modes excited close to the gap edge are considerably modified compared to those obtained in a uniform density disk. We find the torque density in physical space to be more concentrated towards the perturber and different from the uniform disk theory predictions typically by a factor of several in this region. At least for the particular gap profiles considered in this work we find that the torque density at the gap edge drops exponentially with the distance from the perturber (as opposed to the power law scaling expected from uniform disk theory). In parts of the disk where the density is roughly uniform we observe the negative torque density phenomenon in agreement with the results of Dong et al. (2011a) and RP12. Despite these differences in the torque density distribution the total angular momentum flux driven by the perturber through the disk seems to agree with the

existing prescriptions at the level of $\sim 10\%$. The relative perturbation of the surface density is shown to go down in amplitude as the density wave propagates out of the gap, which has important implications for the nonlinear wave evolution and damping.

These results suggest that the process of gap opening in protoplanetary disks and gas clearing around SMBH binaries would be more efficient than the current theory predicts. Our revision of the torque density prescription should have important effect on the self-consistent calculation of the gap density profile and, consequently, on the orbital evolution of the perturber (Type II migration speed for planets and SMBH inspiral rate). Future extension of our results to the full cylindrical geometry will allow direct applications of the non-uniform disk theory to systems with wide gaps or cavities.

The financial support for this work is provided by the Sloan Foundation, NASA grant NNX08AH87G, NSF grant AST-0908269, and CONICYT Bicentennial Becas-Chile fellowship awarded to CP.

REFERENCES

- Alexander, R. D., Smedley, S.L., Nayakshin, S., & King, A. R. 2012, *MNRAS*, 419, 1970
 Armitage, P. J., Livio, M., Lubow, S. H., & Pringle, J. E. 2002, *MNRAS*, 334, 248
 Armitage, P. J. & Natarajan, P. 2002, *ApJ*, 567, L9
 Artymowicz, P. 1993, *ApJ*, 419, 155
 Bate, M. R., Lubow, S. H., Ogilvie, G. I., & Miller, K. A. 2003, *MNRAS*, 341, 213
 Bryden, G., Chen, X., Lin, D. N. C., Nelson, R. P., & Papaloizou, J. C. B. 1999, *ApJ*, 514, 344
 Chang, P., Strubbe, L. E., Menou, K., & Quataert, E. 2010, *MNRAS*, 407, 2007
 Crida, A., Morbidelli, A., & Masset, F. 2006, *Icarus*, 181, 587
 Cuadra, J., Armitage, P. J., Alexander, R. D., & Begelman, M. C. 2009, *MNRAS*, 393, 1423
 D'Angelo, G. & Lubow, S. H. 2008, *ApJ*, 685, 560
 D'Angelo, G. & Lubow, S. H. 2010, *ApJ*, 724, 730
 de Val-Borro M. et al. 2006, *MNRAS*, 370, 529
 Dong, R., Rafikov, R. R., Stone, J. M., & Petrovich, C. 2011, *ApJ*, 741, 56
 Dong, R., Rafikov, R. R., Stone, J. M. 2011, *ApJ*, 741, 57
 Duffell, P. C. & MacFadyen, A. I. 2012, arXiv:1202.5608
 Farris, B. D., Liu, Y. T., & Shapiro, S. L. 2011, *Phys. Rev. D*, 84, 024024
 Goldreich, P. & Tremaine, S. 1980, *ApJ*, 241, 425 (GT80)
 Goldreich, P. & Lynden-Bell, D. 1965, *MNRAS*, 130, 125
 Goldreich, P., & Nicholson, P. D. 1989, *ApJ*, 342, 1075
 Goodman, J. & Rafikov, R. R. 2001, *ApJ*, 552, 793
 Gould, A. & Rix, H.-W. 2000, *ApJ*, 532, L29
 Greenberg, R. 1983, *Icarus*, 53, 207
 Hasegawa, Y. & Pudritz, R. 2011, *MNRAS*, 417, 1236
 Ivanov, P. B., Papaloizou, J. C. B., & Polnarev, A. G. 1999, *MNRAS*, 307, 79
 Korycansky, D. G. & Pollack, J. B. 1993, *Icarus*, 102, 150 (KP93)
 Kocsis, B., Yunes, N., & Loeb, A. 2011, *Phys. Rev. D*, 84, 024032
 MacFadyen, A. I. & Milosavljević, M. 2008, *ApJ*, 672, 83
 Matsumura S., Pudritz R. E., Thommes E. W., 2007, *ApJ*, 660, 1609
 Lin, D. N. C., & Papaloizou, J. C. B. 1979, *MNRAS*, 186, 799
 Lin, D. N. C., & Papaloizou, J. C. B. 1986, *ApJ*, 309, 846
 Liu, Y. T. & Shapiro, S. L. 2010, *Phys. Rev. D*, 82, 123011
 Lodato, G., Nayakshin, S., King, A.R., & Pringle, J.E., 2009 *MNRAS*, 398, 1392
 Lunine, J. I., & Stevenson, D. J. 1982, *Icarus*, 52, 14
 Masset, F. S., Morbidelli, A., Crida, A., Ferreira, J., 2006, *ApJ*, 642, 478
 Masset, F. S. 2011, *Celestial Mechanics and Dynamical Astronomy*, 111, 131
 Menou, K. & Goodman, J. 2004 *ApJ*, 606, 520
 Meyer-Vernet, N. & Sicardy, B. 1987, *Icarus*, 69
 Muto, T. & Inutsuka, S. 2009, *ApJ*, 701, 18
 Narayan, R., Goldreich, P., & Goodman, J. 1987, *MNRAS*, 228, 1 (NGG)
 Papaloizou, J. C. B. & Lin, D. N. C. 1984, *ApJ*, 285, 818
 Rafikov, R. R. 2002a, *ApJ*, 569, 997
 Rafikov, R. R. 2002b, *ApJ*, 572, 566
 Rafikov, R. R. & Petrovich, C. 2012, *ApJ*, 747, 24 (RP12)
 Roedig, C. et al. 2012, arXiv:1202.6063v1
 Shi, J.-M., Krolik, J. H., Lubow, S. H., & Hawley, J. F. 2011, arXiv:1110.4866
 Takeuchi, T., Miyama, S. M., & Lin, D. N. C. 1996, *ApJ*, 460, 832
 Tanaka, H., Takeuchi, T., & Ward, W. R. 2002, *ApJ*, 565, 1257
 Trilling, D. E., Benz, W., Guillot, T., Lunine, J. I., Hubbard, W. B., & Burrows, A. 1998, *ApJ*, 500, 428
 Varnière, P., Quillen, A. C., & Frank, A. 2004, *ApJ*, 612, 1152
 Ward, W. R. 1986, *Icarus*, 67, 164
 Ward, W. R. 1997, *Icarus*, 126, 261

APPENDIX

SHIFTED LINDBLAD RESONANCES IN THE SHEARING-SHEET APPROXIMATION

The angular frequency of the non-uniform isothermal disk in full cylindrical geometry is given by

$$\Omega^2(r) = \Omega_K^2(r) + \frac{c_s^2}{r} \frac{\partial \ln \Sigma_0}{\partial r}, \quad (\text{A1})$$

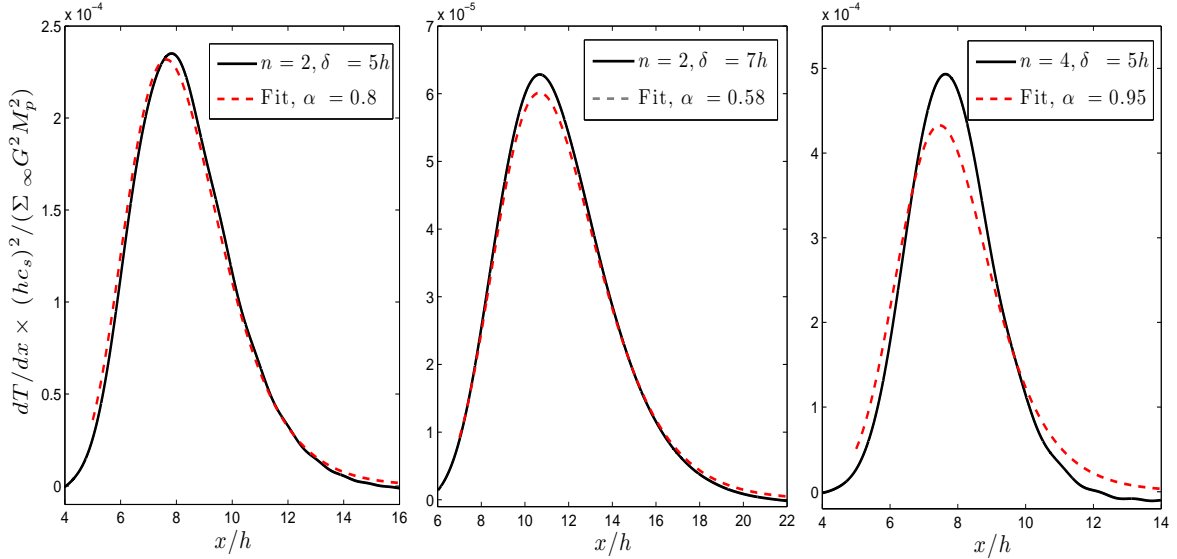


FIG. 9.— Torque density outside the gap for three different models (23) with $\Sigma_{\min} = 3 \times 10^{-4}$, and different n and δ as specified in each panel. Black curves show our numerical results while the red dashed curves show the fit (B1) with the input parameter α indicated in each panel.

where Ω_K is the regular Keplerian frequency. The modified epicyclic frequency is then given by

$$\kappa^2 = 4\Omega^2 + 2r\Omega \frac{\partial \Omega}{\partial r} = \Omega_K^2(r) + c_s^2 \frac{\partial^2 \ln \Sigma_0}{\partial r^2} + \frac{3c_s^2}{r} \frac{\partial \ln \Sigma_0}{\partial r}. \quad (\text{A2})$$

The locations r_L at which the Lindblad resonance condition $m^2 [\Omega(r_L) - \Omega_p]^2 = \kappa^2(r_L)$ (here $\Omega_p \equiv \Omega_K(r_p)$ is the pattern speed of the gravitational perturbation and $m = k_y r_p$ is the wavenumber) are given by the following relation:

$$m^2 \left[\sqrt{\Omega_K^2(r_L) + \frac{c_s^2}{r} \frac{\partial \ln \Sigma_0}{\partial r} \Big|_{r_L}} - \Omega_p \right]^2 = \Omega_K^2(r_L) + c_s^2 \left(\frac{\partial^2 \ln \Sigma_0}{\partial r^2} + \frac{3}{r} \frac{\partial \ln \Sigma_0}{\partial r} \right) \Big|_{r_L}. \quad (\text{A3})$$

Expressing m via k_y we find the following relation between k_y and corresponding r_L , which does not make any approximations and is valid in full cylindrical geometry:

$$k_y(r_L) = \pm \frac{\kappa(r_L)}{\Omega_p r_p} \left[\sqrt{\left(\frac{r_p}{r_L} \right)^3 + \frac{h^2}{r} \frac{\partial \ln \Sigma_0}{\partial r} \Big|_{r_L}} - 1 \right]^{-1}, \quad \kappa^2(r_L) = \Omega_p^2 \left[\left(\frac{r_p}{r_L} \right)^3 + h^2 \left(\frac{\partial^2 \ln \Sigma_0}{\partial r^2} + \frac{3}{r} \frac{\partial \ln \Sigma_0}{\partial r} \right) \Big|_{r_L} \right]. \quad (\text{A4})$$

In the shearing sheet approximation one takes $r_L = r_p + x_L$, expands r_p/r_L to linear order in x_L/r_p and then takes the limit $r_p \rightarrow \infty$. As a result one recovers the resonance condition in the form (24) with κ given by equation (25).

A ONE-PARAMETER TORQUE DENSITY FIT

Given the numerical challenges involved in the calculation of the torque density in a general non-uniform disk we try to provide an empirical fit for dT/dx . Our procedure is based on the following logic.

For every gap model considered in this work we find that the torque density per unit surface density Σ_0 decays exponentially outside the gap until it becomes negative because of the negative torque density phenomenon (RP12). In particular, for our fiducial model the fall-off is described reasonably well by $\exp(-0.8x/h)$ for $x/h > 5$ as shown in Figure 6. Also, as discussed in §6.2, 7 the full integrated torque $T(\infty)$ coincides within $\sim 10\%$ with the prediction based on simple GT80 prescription (4) and (32). We use this property to get a normalization to the exponential fall-off outside the gap. Putting these two ideas together we come up with the following fit for the torque density outside the gap ($x > \delta$):

$$\frac{dT}{dx} = C(\alpha) \text{sign}(x) \frac{(GM_p)^2 \Sigma_0(x)}{\Omega^2 h^4} e^{-\alpha x/h}, \quad C(\alpha) = 2.5 \frac{\int_{\delta}^{\infty} \Sigma_0(x) / (x/h)^4 dx}{\int_{\delta}^{\infty} \Sigma_0(x) e^{-\alpha x/h} dx}, \quad (\text{B1})$$

where α is a dimensionless free parameter that controls the exponential fall-off and takes value in the range $\sim 0.5 - 1$ for all our numerical calculations as we show next.

In Figure (9), we show how this fit performs for different gap profiles as we vary the width or steepness of the density profiles (the torque density outside the gap does not depend on its density contrast Σ_{\min} , see §7.3). In the left panel, we consider our fiducial model and the fitting formula using $\alpha = 0.8$. Our prescription fits the numerical result pretty

well from $5h \lesssim x \lesssim 15h$, while beyond $15h$ the torque density becomes negative and the correct asymptotic behavior is given by the analytical expression $-0.63\Sigma_0(x)/x^4$, see RP12 (in proper units).

In the middle panel, we increase the width of the gap by taking $\delta = 7h$ and show a fit with $\alpha = 0.58$, which works well for $7h \lesssim x \lesssim 22h$, before torque density changes sign.

In the right panel, we increase the steepness of the gap profile by using $n = 4$ and show the best fit (B1), which now requires $\alpha = 0.95$. In this case, the fit is worse than in the previous examples with relative errors up to $\lesssim 20\%$ at the peak of the torque density, but it still does a better job than the asymptotic expression from GT80.

Unfortunately, at the moment we cannot predict a value of the parameter α featured in equation (B1) for a particular gap profile. But the results shown in Figure 9 suggest that the torque density decay is faster and the fits demands higher values of α for boxier density profiles (i.e. for higher n) and for narrower gaps (i.e. for lower δ).